AIAA JOURNAL
Vol. 44, No. 8, August 2006

Modeling of Wake-Induced Transition in Linear Low-Pressure Turbine Cascades

S. Lardeau* and M. A. Leschziner†
Imperial College London, London, England SW7 2AZ, United Kingdom

An unsteady Reynolds-averaged Navier–Stokes (URANS) strategy is applied to the problem of wake-induced transition at high freestream turbulence on the suction side of two blades representative of those used in low-pressure turbines. Experimentally, the blades are arranged in high-aspect-ratio linear cascades, with upstream circular bars generating passing wakes, and two-dimensional flow conditions are, thus, assumed. The strategy combines an explicit algebraic Reynolds-stress turbulence model with transition-specific modifications targeted at capturing the effects of high freestream turbulence and of pretransitional laminar fluctuations. Close attention is paid to numerical accuracy, and grids of up to 140,000 cells are used in combination with 800 time steps per pitchwise traverse to resolve small-scale features in the blade boundary layers that are associated with the unsteady interaction. The computational results demonstrate that the combined model returns a good representation of the response of the suction-side boundary layer to the passing wakes in both blades. Specifically, in the boundary layer of one of the two blades, the wakes are observed to cause a periodic upstream shift in the transition onset and, thus, correspondingly periodic attachment and calming. In the other, no separation occurs, and the wakes are shown to produce a significant periodic reduction in shape factor and increase in skin friction in the blade boundary layer, again as a consequence of the upstream shift in the transition location.

Nomenclature

a_{ij}	=	anisotropy tensor
C	=	blade-chord length
D	=	diameter of the bar
f_ω	=	wall-damping function
H	=	shape factor, δ_1/δ_2
k	=	turbulence energy
n^*	=	nondimensional wall distance, $u_\varepsilon n/\nu$
Re_t	=	turbulent Reynolds number, $k^2/\nu\varepsilon$
S_{ij}	=	strain tensor
s	=	coordinate along the suction side of the blade
T	=	period for one passage of the bar
Tu	=	turbulence intensity
U_b	=	streamwise velocity of the incoming flow
$\overline{u_i u_j}$	=	stress tensor
u_ε	=	Kolmogorov velocity scale, $(\nu\varepsilon)^{1/4}$
V_x	=	vertical velocity of the moving bar
δ_1	=	displacement thickness
δ_2	=	momentum thickness
ε	=	dissipation rate of turbulence energy
ν	=	viscosity
ν_t	=	turbulent viscosity
Ω_{ij}	=	vorticity tensor
ω	=	specific dissipation rate, ε/k

I. Introduction

UNSTEADY wake–blade interaction is an inevitable consequence of the relative motion between rotors and stators in turbomachines. This interaction is multifaceted, involving both potential (pressure-induced) and viscous (turbulent) components, and is of considerable practical interest. Although it might be supposed that the interaction has only negative consequences (noise, vibrations, added total pressure losses through turbulence and flow distortions), it can, in fact, have important benefits to the operational characteristics of turbine blades. The flow in a low-pressure stage has a relatively low Reynolds number, of order 10^5, based on chord length, and a substantial proportion of the boundary layer on the blade surface is, thus, laminar or transitional. Whereas the flow in a turbine accelerates, globally, the middle-to-rear portion of the suction side of a highly loaded turbine blade is subjected to an adverse pressure gradient. This can easily lead, especially in laminar and transitional conditions, to separation and, thus, to a serious deterioration in performance. In this environment, the introduction of unsteady wakes reduces the trend toward boundary-layer separation, in a time-mean sense, by way of two processes. First, the wake introduces dynamic perturbations to the boundary layer, which result in a correspondingly periodic upstream shift of the transition location, eliminating separation for a proportion of the wake-sweep period. In one proposed scenario, the leading edge of the wake provokes, as it sweeps along the suction side, the formation of unsteady rollup vortices in the laminar boundary layer, which initiate transition and then move upstream as turbulent or transitional structures, thus suppressing separation. Second, the wake transports turbulence toward the suction-side boundary layer. This turbulence is further enhanced by local straining, associated with shear within the wake and additional strains generated by the distortions in the passage flow. The proximity of the turbulent wake to the boundary layer then favors an early onset of bypass transition, both by the penetration of pressure fluctuations and diffusion of turbulence energy into the boundary layer, thereby enhancing its ability to resist separation. The two processes are, thus, mutually supportive in causing the boundary layer to undergo unsteady transition at a location that shifts periodically upstream along the suction side as a wake passes over the blade. In between consecutive wakes, the boundary layer relaxes toward an unperturbed state, with a substantial turbulent stretch on the rear suction side, a condition referred to as *calming*. Thus, in the mean, separation is reduced, if not entirely eliminated, the global consequence being a reduction of total pressure losses by as much as 25%.

The transitional aspects identified in the foregoing paragraph makes the computational prediction of wake–blade interaction an especially challenging task. The transition process is preceded by the growth of instabilities, whether transition is natural, following

Received 6 March 2005; revision received 3 February 2006; accepted for publication 16 February 2006.

*Research Associate, Department of Aeronautics, Prince Consort Road, South Kensington.

†Professor, Department of Aeronautics, Prince Consort Road, South Kensington.

laminar separation provoked by wake dynamics, or of the bypass type, initiated by high freestream turbulence in attached conditions. In the latter case, the one more pertinent to turbomachinery, both simulations[1] and experiments[2] show that the boundary layer contains a substantial level of (pseudoturbulent) fluctuations well before the boundary layer bursts into a truly turbulent state, at which point the skin friction rises rapidly and the shape factor drops correspondingly. Simulations[3,4] show, furthermore, that the pretransitional turbulence is characterized by almost one-dimensional fluctuations associated with elongated wavy structures, so that turbulent mixing by cross correlations—that is, shear stress—is weak. Finally, simulations suggest that pressure fluctuations outside the boundary layer, as well as anisotropy in the turbulent fluctuations in the freestream, have a strong effect on the manner in which transition is initiated.

Most of the described transitional features cannot be represented in a physically meaningful manner by any Reynolds-averaged modeling strategy. At best, conventional turbulence-transport models account for the process of turbulence diffusion from the freestream into the boundary layer, favoring bypass transition, and the opposing effect of viscosity-containing damping terms, effective in the viscous near-wall layer. Transition is then mimicked as a bifurcation of the mathematical system constituting the turbulence model, this bifurcation reflecting amplification by turbulence generation exceeding damping by dissipation. How this takes place, given a set of flow conditions, depends greatly on the closure assumptions built into the model. Numerous studies, most summarized in reviews by Savill,[5,6] demonstrate that many low-Reynolds-number models applied to bypass transition return a broadly correct transition-onset location, identified by the sharp rise in skin friction, in a zero-pressure-gradient flat-plate boundary layer, but that most models fare badly in more complex conditions, returning indifferent or erroneous responses to variations in freestream turbulence, pressure gradient, and wall curvature.

A popular alternative strategy to using low-Reynolds-number models is to delegate the prediction of the transition onset to a separate transition model and to switch to a conventional turbulence model once transition has occurred. With this combination, the turbulence model plays no part in the transition process itself and need not contain wall-damping terms. Transition is characterized, in most approaches, by an intermittency parameter, $0 < \gamma < 1$ (Mayle[7]), that identifies the fraction of time over which the flow, at any given spatial location, is turbulent. The distribution of γ, either as a one-dimensional property along the boundary layer or as field also accounting for transverse variations, can be derived from one of a number of models proposed, some consisting of algebraic correlations derived from experimental data[8,9] and others involving an evolution equation that aims to account for the transport of the intermittency,[10–15] with the rate of generation typically leaning on various elements used in the algebraic correlations: for example, the spot-production rate. Once γ is determined, it is used either within conditionally averaged Navier–Stokes equations (see Steelant and Dick[11,12]) or by simply multiplying the eddy viscosity by γ in the mean-flow equation. In the pretransitional regime, γ is set to zero, and it is only assuming a positive value when the model is required to initiate transition. Although such models can be made to perform reasonably well, they are highly pragmatic and empirical in nature, do not resolve potentially important near-wall processes, do not account for pretransitional phenomena, and are not readily extendible to unsteady conditions.

A recent study by Lardeau et al.[16] addresses the question of how conventional turbulence models can be combined with an intermittency-type approximation and a component for pretransitional fluctuations to yield a modeling framework that is superior to those outlined earlier and more generally applicable. The cornerstone of this framework is the low-Reynolds-number explicit algebraic Reynolds-stress model of Abe et al.[17] (AJL model). This model distinguishes itself from others in the same category by returning correctly all of the Reynolds-stress components as the wall is approached, including the wall-asymptotic limit. This is, arguably, an important property in flows in which near-wall processes play an influential role in both the transition and posttransition regions, as well as for heat transfer predictions. Second, the model is applicable to a larger range of complex turbulent-flow conditions by virtue of its anisotropy-resolving properties. When operating on its own, the model is found to give premature transition and not to respond well to variations of freestream turbulence and pressure gradient, not an unusual observation with most models of this type. Lardeau et al.[16] then proceeded to introduce two transition-specific elements into the turbulence model, one describing the evolution of the pretransitional fluctuation energy and the other an intermittency-type correlation, to control the turbulent viscosity returned by the default AJL model. The details follow subsequently. Lardeau et al.[16] show that the resulting model performs well in transitional, statistically steady flat-plate boundary layers in variable pressure gradient and on a von Kàrmàn Institute (VKI) turbine blade. Lardeau and Leschziner[18] have also used the baseline model, without transition modifications, to compute unsteady wake–blade interaction in a linear cascade of low-pressure turbine blades (denoted T106), investigated experimentally by Stieger and Hodson.[19,20] In this configuration, the inlet freestream-turbulence intensity was only 1%. However, the transition modifications introduced to the baseline model apply only to elevated freestream turbulence at which bypass transition may be assumed to be the primary effective mechanism. This is the reason why use of the transition modifications was not regarded as being appropriate in that case. The present paper now reports the application of the extended model to two new configurations for which experimental data have only recently emerged and in which the freestream-turbulence level is much higher, namely, 4%, closer to realistic operating conditions. One set of data pertains, again, to the linear cascade considered earlier; the other is for an entirely different blade geometry with a much more rounded leading edge, investigated by Elsner et al.[21] The experimental observations suggest significant differences in the detailed mechanisms of bypass transition and their effects. Hence, taken together, the two configurations represent a searching test of the present transition-modified model.

II. Turbulence Modeling and Computational Approach

For reasons already outlined, the nonlinear eddy-viscosity model (strictly, an explicit algebraic Reynolds-stress model) proposed by Abe et al.[17] has been adopted as the main element of the turbulence-modeling strategy. Apart from its ability to return an exceptionally good representation of the near-wall anisotropy, the choice is motivated by the model's demonstrably good predictive performance for flow separating from curved surfaces,[22] in which the near-wall behavior is influential. This is pertinent to the present application, because the wakes provoke unsteady separation over the curved suction side of the blades under consideration.

Two principal versions of this model exist, one involving a length-scale-related equation for the dissipation rate ε and the other an equation for the specific dissipation $\omega = \varepsilon/k$. The former performs better for transitional flow and has, therefore, been preferred in this study.

The ε version of the model adopts a four-part representation of the effects of strain, vorticity, and wall-proximity on the anisotropy tensor,

$$a_{ij} = \overline{u_i u_j}/k - \tfrac{2}{3}\delta_{ij} = (2/C_D)\left\{c^*_{ij} + [1 - f_w(26)]\left(d^*_{ij} + e^*_{ij}\right) + C_D f_w(26) f^*_{ij}\right\} \quad (1)$$

in which c^*_{ij} relates linearly to the strain tensor, d^*_{ij} includes quadratic terms in strain and vorticity tensors, e^*_{ij} is a term accounting specifically for strong normal straining, and f^*_{ij} relates to wall proximity and orientation. The last term is an especially important fragment, in so far as it is instrumental in securing the correct wall-asymptotic behavior of the anisotropy. In Eq. (1), f_w is the wall-related

damping function

$$f_w(A) = \exp[-(n^*/A)^2] \tag{2}$$

where $n^* = u_\varepsilon n/\nu$ is the nondimensional wall distance and $u_\varepsilon = (\nu\varepsilon)^{1/4}$ is the Kolmogorov velocity scale.

The terms appearing in Eq. (1) are as follows:

$$c^*_{ij} = -C_B S^*_{ij}$$

$$d^*_{ij} = C_B\left[-2\left(S^*_{ik}\Omega^*_{kj} - \Omega^*_{ik}S^*_{kj}\right) + 2\left(S^*_{ik}S^*_{kj} - \frac{\delta_{ij}}{3}S^{*2}\right)\right]$$

$$e^*_{ij} = -C_B f_{s_1} S^*_{ij} + 2C_B f_{s_2}\left(S^*_{ik}S^*_{kj} - \frac{\delta_{ij}}{3}S^{*2}\right)$$

$$f^*_{ij} = -\alpha_\omega \frac{1}{2}\left(d_i d_j - \frac{\delta_{ij}}{3}\right) + \left(1 - fr_1^2\right)\left[\frac{-\beta_\omega C_\omega}{1 + C_\omega\sqrt{S^{**^2}\Omega^{**^2}}} \times \left(S^{**}_{ik}\Omega^{**}_{kj} - \Omega^{**}_{ik}S^{**}_{kj}\right) + \frac{\gamma_\omega C_\omega}{1 + C_\omega S^{**^2}}\left(S^{**}_{ik}S^{**}_{kj} - \frac{\delta_{ij}}{3}S^{**^2}\right)\right]$$

$$C_B = 1\Big/\left\{1 + \frac{22}{3}\Omega^{*2} + \frac{2}{3}\left[\Omega^{*2} - S^{*2}\right][1 + 100(\Omega^* - S^*)]\right\} \tag{3}$$

where

$$S^*_{ij} = C_D\tau S_{ij}, \qquad \Omega^*_{ij} = C_D\tau\Omega_{ij}, \qquad S^{**}_{ij} = \tau_d S_{ij}$$

$$\Omega^{**}_{ij} = \tau_d\Omega_{ij}, \qquad C_D = 0.8 \tag{4}$$

$$S^{*2} = S^*_{mn}S^*_{mn}, \qquad \Omega^{*2} = \Omega^*_{mn}\Omega^*_{mn}, \qquad S^{**^2} = S^{**}_{mn}S^{**}_{mn}$$

$$\Omega^{**^2} = \Omega^{**}_{mn}\Omega^{**}_{mn}, \qquad S^* = \sqrt{S^{*2}}, \qquad \Omega^* = \sqrt{\Omega^{*2}} \tag{5}$$

$$f_{s_1} = f_{r_1}f_{r_2}15\left(\Omega^{*2} - S^{*2}\right), \qquad f_{s_2} = -f_{r_1}f_{r_2}\left[1 + 7\left(\Omega^{*2} - S^{*2}\right)\right] \tag{6}$$

$$f_{r_1} = \left(\Omega^{*2} - S^{*2}\right)\Big/\left(\Omega^{*2} + S^{*2}\right), \qquad f_{r_2} = S^{*2}\Big/\left(\Omega^{*2} + S^{*2}\right) \tag{7}$$

The set of coefficients are those given by Abe et al.[17]:

$$\alpha_\omega = 1, \qquad \beta_\omega = \tfrac{1}{4}, \qquad \gamma_\omega = 1.5, \qquad C_\omega = 0.5 \tag{8}$$

The term d_i represents the wall-normal direction. In the work of Abe et al.,[17] this term is based on the wall distance n, and it takes the form

$$d_i = \frac{N_i}{\sqrt{N_k N_k}}, \qquad N_i = \frac{\partial n}{\partial x_i} \tag{9}$$

Finally, the time scale τ_d combines the turbulent macroscale and the Kolmogorov scale,

$$\tau_d = [1 - f_\omega(15)](k/\varepsilon) + f_\omega(15)\sqrt{\nu/\varepsilon} \tag{10}$$

In this formulation, use is made of the turbulence energy k and the dissipation rate ε to achieve the requisite dimensional consistency in Eq. (1).

In constructing a specific transition model, based on the previous nonlinear stress–strain relationship, Lardeau et al.[16] proposed that, in the transitional region, the total turbulence energy k is a combination of the laminar fluctuations energy k_l and the conventional turbulence energy k_t. The total turbulence energy is then given by $k = (1-\gamma)k_l + \gamma k_t$, where γ is a function varying between 0 in the laminar region and 1 in the fully turbulent flow.

The specific transition model also requires a new definition for the turbulent viscosity, given by

$$\nu_t = c_\mu f_\mu[k(\gamma k_t)/\varepsilon] \tag{11}$$

from which the time scale $\tau = \nu_t/k$ is obtained. The damping function

$$f_\mu = \left\{1 + \left(35\Big/Re_t^{\frac{3}{4}}\right)\exp\left[-(Re_t/30)^{\frac{3}{4}}\right]\right\}[1 - f_w(26)] \tag{12}$$

represents the influence of fluid viscosity on its turbulent counterpart. The variable γ appearing in Eq. (11) may be regarded as an intermittency parameter. The present approach to its quantification leans heavily on the correlation of Dhawan and Narasimha,[8] which relates the transition-onset location to the Reynolds number, a (turbulent) spot-formation rate and a spot-propagation parameter. A variation of the preceding correlation that has been found to perform well in combination with the present nonlinear eddy-viscosity model is the following:

$$\gamma = 1 - f_\omega(26)\left[-Re_{s_b}^2\hat{n}\sigma\right] \tag{13}$$

where $Re_s = (s - s_b)U_i n/\nu$ is the local Reynolds number, based on the distance from the transition onset of the blade and on the local freestream velocity (relative to the blade velocity). The values of $\hat{n}$ and of σ (respectively, the dimensionless spot-formation rate and the spot-propagation parameter) are given for zero pressure gradient by Mayle[7] as

$$\hat{n}\sigma = 1.25 \times 10^{-11} Tu^{-\frac{7}{4}} \tag{14}$$

and, when the flow is submitted to pressure gradient, by

$$\frac{\hat{n}\sigma}{(\hat{n}\sigma)_{ZPG}} = \begin{cases} (474Tu^{-2.9})^{1-\exp(2\times 10^6 K)}, & \text{for } K < 0 \\ 10^{-3227K^{0.5985}}, & \text{for } K > 0 \end{cases} \tag{15}$$

where $(\hat{n}\sigma)_{ZPG}$ is calculated using expression (14), K is the acceleration parameter $[K = (\nu/U^2)(\mathrm{d}U/\mathrm{d}x)]$ and Tu is the freestream-turbulence intensity. The location of the transition onset is computed using Mayle's correlation $Re_{\theta_b} = 400Tu^{-0.625}$, with θ_b being the momentum thickness at the location s_b.

An issue to highlight is that Eq. (13) is not Galilean invariant. This is an inevitable consequence of the adoption of an algebraic intermittency model that correlates the transition onset to the Reynolds number, in a manner similar to that done extensively in the past. Note, however, that, outside the transitional region, Eq. (13) changes rapidly between the limiting values 0 in the laminar region and 1 in the turbulent one, so that the solution outside the thin transitional region does not depend on the computation of γ. It would be possible, in principle, to devise a differential form of Eq. (13), that is, an evolution equation for γ. However, this is a separate modeling effort and would involve extensive additional calibration in combination with the present nonlinear eddy-viscosity model.

The turbulence energy and its dissipation are derived, respectively, from

$$\frac{\mathrm{D}k_t}{\mathrm{D}t} = \frac{\partial}{\partial x_j}\left[\left(\nu + \frac{\nu_t}{\sigma_k}\right)\frac{\partial k_t}{\partial x_j}\right] - \underbrace{\overline{u_i u_j}\frac{\partial U_i}{\partial x_j}}_{P_k} - \varepsilon \tag{16}$$

$$\frac{\mathrm{D}\varepsilon}{\mathrm{D}t} = \frac{\partial}{\partial x_j}\left[\left(\nu + \frac{\nu_t}{\sigma_\varepsilon}\right)\frac{\partial \varepsilon}{\partial x_j}\right] - c_{\varepsilon_1}\frac{\varepsilon}{k_t}\overline{u_i u_j}\frac{\partial U_i}{\partial x_j} - c_{\varepsilon_2}f_\varepsilon\frac{\varepsilon^2}{k_t} \tag{17}$$

where

$$\sigma_k = 1.2/f_t, \qquad f_t = 1 + 5.0 f_w(5) \tag{18}$$

$$f_\varepsilon = \left\{1 - 0.3\exp\left[-(Re_t/6.5)^2\right]\right\}[1 - f_w(3.7)]$$

$$c_\mu = 0.12, \qquad c_{\varepsilon_1} = 1.45, \qquad c_{\varepsilon_2} = 1.83, \qquad \sigma_\varepsilon = 1.5/f_t \tag{19}$$

Following Mayle and Schulz[23] and Lardeau et al.,[16] the laminar-kinetic-energy equation is given by

$$\frac{\mathrm{D}k_l}{\mathrm{D}t} = C_\omega \frac{U_\infty^2}{\nu}\sqrt{k.k_\infty}\exp\left(\frac{-y^+}{13}\right) + \nu\frac{\partial^2 k_l}{\partial n^2} - 2\nu\frac{k_l}{n^2} \qquad (20)$$

where C_ω depends on the effective frequency and the turbulence level in the freestream and k_∞ is the level of k at the edge of the boundary layer.

In a previous study, Lardeau and Leschziner[24] show that wake-induced transition on the same T106A blade as that considered here, but at low freestream turbulence (less than 1%), is well represented by the baseline turbulence model itself. The reason for this favorable performance is a matter of debate. Hodson and Howell[2] argue that both velocity deficit and high turbulence energy within the wake can induce transition. Because both mechanisms occur simultaneously, a distinction of the two causes is difficult. However, the model itself only induces transition in response to the interaction between the boundary layer and the turbulence "cloud" transported toward the boundary layer within the wake. On the other hand, the present turbulence model, when combined with the transition-specific elements, performs well for a high value of Tu (higher than 1%) in steady cases.[16] Hence, here, the major role of the specific transition modification is to enhance the predictive realism of the transition in the flow between the wakes. Based on this argument, the implementation of the transition model for the present unsteady conditions follows the one proposed for a flow over a blade in steady conditions by Lardeau et al.[16] Hence, the values of the spot-propagation σ and the spot-production rate $\hat{n}$ used in Eq. (13) are those used in steady conditions.

The computational strategy is a multiblock version of the nonorthogonal, fully collocated, finite volume scheme STREAM by Lien et al.[25] This original version has been extended by Chen and Leschziner[26] to accommodate relative bar–blade movement by way of a sliding–mesh methodology. However, this capability is not exploited here directly to compute the actual interaction process, for reasons justified in previous papers[18] in which comparative computations, with and without the moving bar included in the computational solution, are discussed. Rather, the wake approaching the blades is prescribed along a plane upstream of the blades, a practice explained later in more detail. Convection of all transported properties is approximated using the UMIST–total variation diminishing scheme,[27] and time marching is performed with a second-order scheme. The SIMPLE pressure-correction algorithm is used to enforce mass conservation within any one time step, by means of an in-step iteration.

III. Flow Configurations

Two different blade geometries have been computed, for both of which experimental data are available. The first blade, designated T106, has been studied experimentaly by Opoka and Hodson,[28] whereas the second blade, TC4, has been studied by Elsner et al.[21]

The blades are shown in Fig. 1, both having profiles used in low-pressure (LP) stages. The main geometric and flow parameters are listed in Table 1. Figure 1 indicates the domains of solution and the grid topology (only every fourth gridline is shown). In both cases, the domain extends over one pitchwise periodic segment. The grid is formed with 12 blocks, the block closest to the blade having an O topology and being close to orthogonal. The total number of cells is 141,000 in both cases, with a value of y^+ below 1 on both sides of the turbine blade.

As demonstrated by Lardeau and Leschziner,[18] this high number of cells (within a two-dimensional representation) is necessary to avoid a significant level of numerical error in this type of flow in which a principal computational challenge is to represent faithfully the convection of time-changing scalar turbulence quantities across a highly skewed grid over a large domain and a substantial period of time. To illustrate the need for care in relation to numerical accuracy, Fig. 2 shows computed contours of a passive scalar cloud convected (with physical diffusion nullified) across a flat plate placed in a variable-area channel, which provokes a pressure field on the plate that mimics the field acting on the suction side of an LP turbine blade. This geometry (but involving actual wakes generated by moving bars) was investigated experimentally by Stieger and Hodson.[20] Computational results are included here for two different grid densities, 43,500 cells and 215,000 cells, respectively. For this passive-scalar demonstration, a steady flowfield has been computed, and this is frozen during the unsteady convection of the cloud. The inlet value of the scalar property within the cloud is 1, and this value should be maintained in the cloud in the absence of any

Table 1 Parameters for the blade cascade

Parameter	T106A	TC4
Chord length C, mm	198	300
Axial chord length	$0.8585C$	$0.7C$
Reynolds number Re_C	0.97×10^5	3.2×10^5
Blade pitch	$0.798C$	$0.8C$
Distance bar to L.E.	$0.35C$	$0.247C$
Bar pitch	$0.798C$	$0.8C$
Bar diameter	$0.01C$	$0.013C$
Flow coefficient V_x/U_b	0.83	0.85
Freestream turbulence intensity Tu,%	4	4

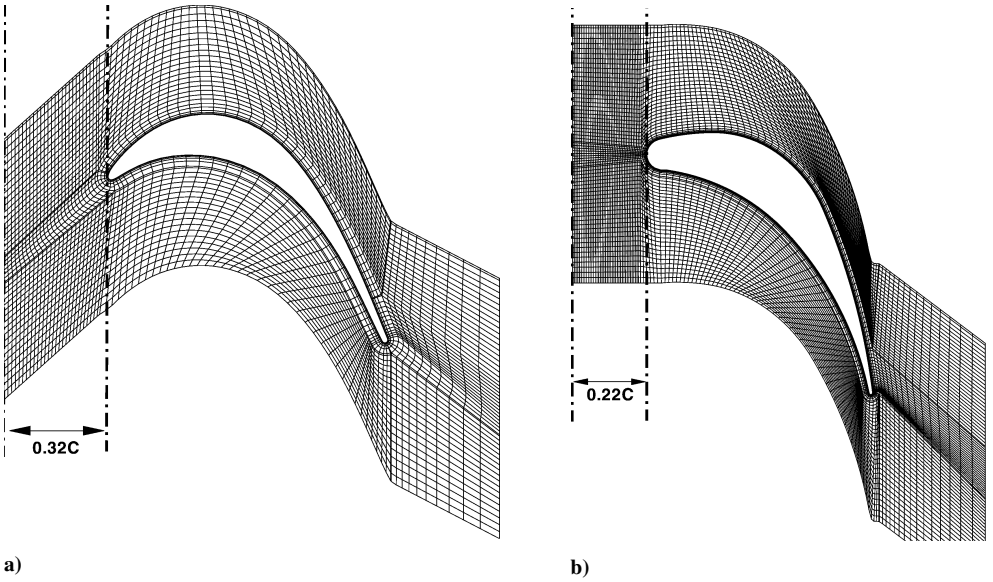

Fig. 1 Computational domains: a) T106A test case and b) TC4 test case.

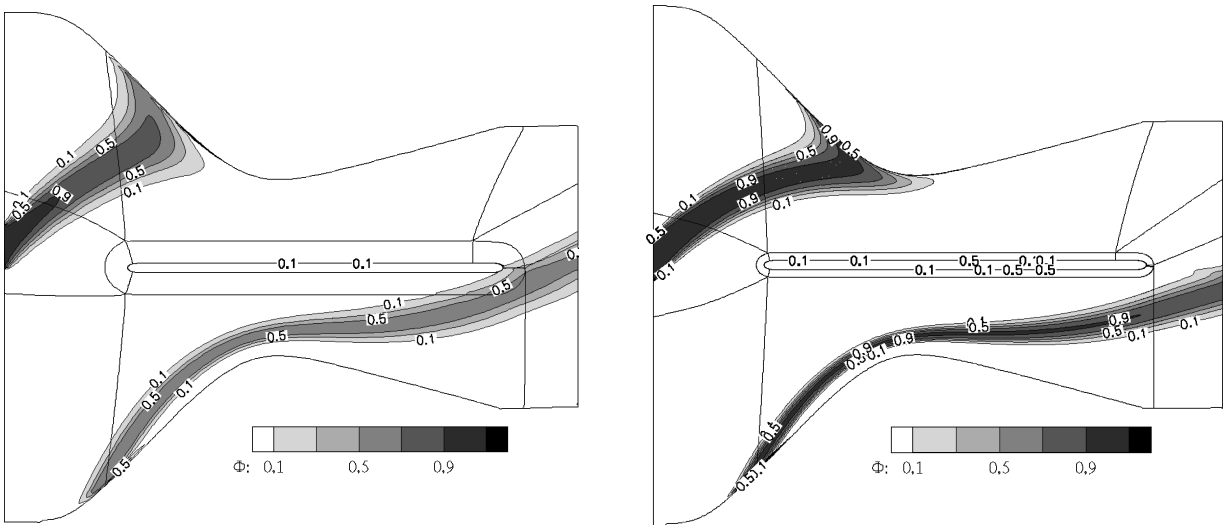

a) $n_t = 400$, $n_{\text{cells}} = 40{,}200$ b) $n_t = 800$, $n_{\text{cells}} = 245{,}900$

Fig. 2 Snapshots of isocontours of passive scalar transported past a ducted flat plate for two grids: n_t = number of time steps per pitchwise traverse and n_{cells} = number of cells for two-dimensional simulation.

numerical diffusion. As is evident, however, numerical diffusion is high at the lower resolution, the scalar value dropping below 0.5 at the outlet, whereas the value remains close to 1 at the higher resolution. Note that this test is numerically more challenging than resolving the real case of a turbulent wake propagating through the blade passage, for in that case turbulence is generated in the passage, due to straining, dissipated and diffused.

The inflow conditions were prescribed at $0.32C$ and $0.22C$ upstream of the blade's leading edge for the T106A and TC4 test cases, respectively. These locations are at three bar diameters downstream of the bar, and the choice of this value is closely linked to the manner in which the bar–wake conditions were generated. In the absence of experimental data on the wake structure in the region between the bar and the blade passage, a precursor simulation was performed, for each case, with a full bar–blade domain discretized with a grid and with a time step fine enough to secure a time- and space-independent solution. A time-averaged solution of the wake was then computed in a moving frame of reference attached to the cylindrical bar, at 3 cylinder diameters downstream of the bar. These time-averaged data were then used at the inlet plane of the final simulation, in the domain shown in Fig. 1. A justification for this process and the choice of 3 bar diameters is given by Lardeau and Leschziner.[18] Briefly, they show that a two-dimensional unsteady Reynolds-averaged Navier–Stokes (URANS) calculation in the manner performed for a cylinder yields a solution that is close to that derived from large eddy simulation (LES), but only in the near field of the cylinder. Beyond 3–4 cylinder diameters, significant discrepancies occur in the structure of the wake, due to a misrepresentation of the interaction between large-scale eddies associated with shedding and the stochastic turbulence. This is also why a full, interactive bar–blade computation is not appropriate. The dissipation rate within the inlet wake was then estimated from the mixing-length relationship

$$\varepsilon_{in} = c_\mu^{\frac{3}{4}} \left(k^{\frac{3}{2}} \Big/ l_{\text{mix}} \right) \tag{21}$$

where $l_{\text{mix}} = \alpha\delta$ is the mixing length for a wake, α is equal to 0.18 (Wilcox[29]), and δ is the half-width of the wake. Outside the wake, the freestream-turbulence level is fixed at the experimentally given value of 4%, whereas the inlet dissipation rate has been estimated by a trial-and-error matching of the decay of the freestream turbulence within the passage to the experimentally observed variation.

IV. Results

A. Blade T106A

The principal indicators of transition are the shape and friction factors, and it is their variation in time and space that provides the bulk of the information that identifies the effects of the passing wakes on the boundary layer. Other informative indicators include the temporal variation of the maximum/minimum velocity at the edge of the boundary layer and the turbulence energy. Thus, space–time plots of these quantities are shown in Figs. 3–6, which cover three pitch periods. Four lines are included in Figs. 3–6; three straight and the fourth undulating: line A marks the locus of peak velocity at the edge of the boundary layer; line B indicates the center of the wake (where the velocity deficit is maximum); line E identifies the locus of minimum velocity occurring between two neighboring wakes; line F (broadly vertical) varies in time around $S/S_{\max} = 0.6$ and indicates the location of transition as predicted by Mayle's[7] correlation. For the present case, with a given freestream-turbulence intensity at the passage inlet of 4%, this correlation predicts transition to occur at $Re_\theta = 205$.

Figure 3 shows the space–time plot of the velocity perturbation at the edge of the boundary layer, defined as the difference between the boundary-layer-edge velocity and the time-averaged velocity measured at that same location. Figure 3 includes predicted results with and without the transition modification, both showing the maximum fluctuation level to be of order 20%. As expected, the difference is small, because the dynamic processes at the edge of boundary layer are dictated, primarily, by the structure of the wake approaching the boundary layer, rather than the transitional representation. The shape of line F shows a greater sensitivity to the modification, and this reflects the influence of the transition modification on the boundary-layer structure.

The space–time plots of the shape factor, Fig. 4, show that the transition modification has a major influence on the detailed response of the boundary layer to the wake. First, the transition model tends to delay the transition onset, the flow effectively remaining laminar between the wakes (line A). Second, the separation zone, occurring between lines A and B from $S/S_{\max} \approx 0.7$, is extended. Whereas both the original model and its transition-modified form predict wake-induced transition under the passing wakes (between lines B and E), the latter produces a downstream shift, to around $S/S_{\max} \approx 0.8$, in good agreement with the experimental observation. A significant point of difference between the prediction and the experiment relates, however, to features C and D in Fig. 4. These identify short-lived and small separation zones that precede transition. Although it is not possible to offer a definitive explanation of the origin of these features, shown more clearly later by reference to velocity fields, it is entirely possible that they are associated with Kelvin–Helmholtz instabilities. Indeed, Opoka et al.[28] report, based on laser Doppler anemometer data and hot-film measurements not available at the time of writing, that weak rollers of this type are observed at positions and times very close to those predicted. However,

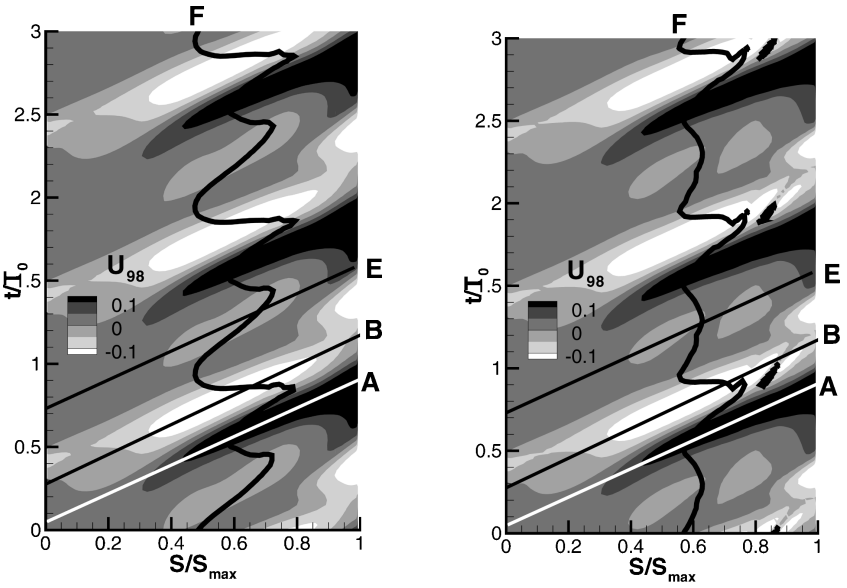

a) Original AJL model b) Specific transition modification

Fig. 3 Space–time plots of velocity perturbations at the edge of the boundary layer, T106A test case, $Tu = 4\%$.

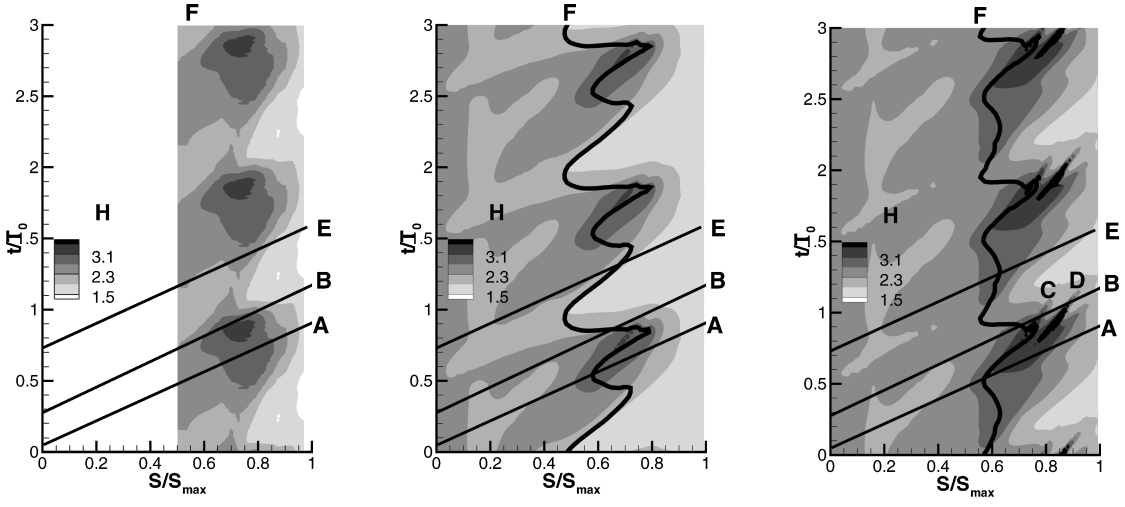

a) Experiment b) Original AJL model c) Specific transition modification

Fig. 4 Space–time plots of the shape factor H, T106A test case, $Tu = 4\%$.

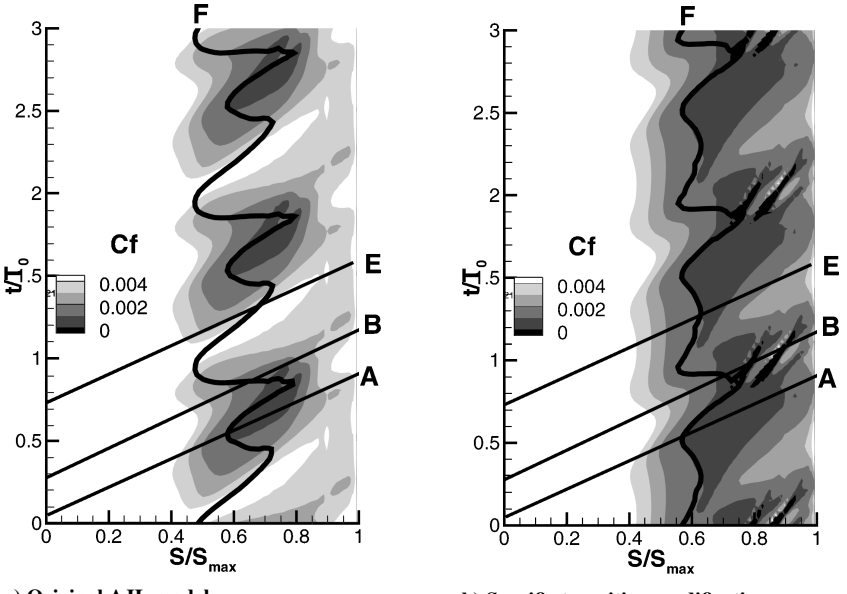

a) Original AJL model b) Specific transition modification

Fig. 5 Space–time plots of the skin-friction coefficient C_f, T106A test case, $Tu = 4\%$.

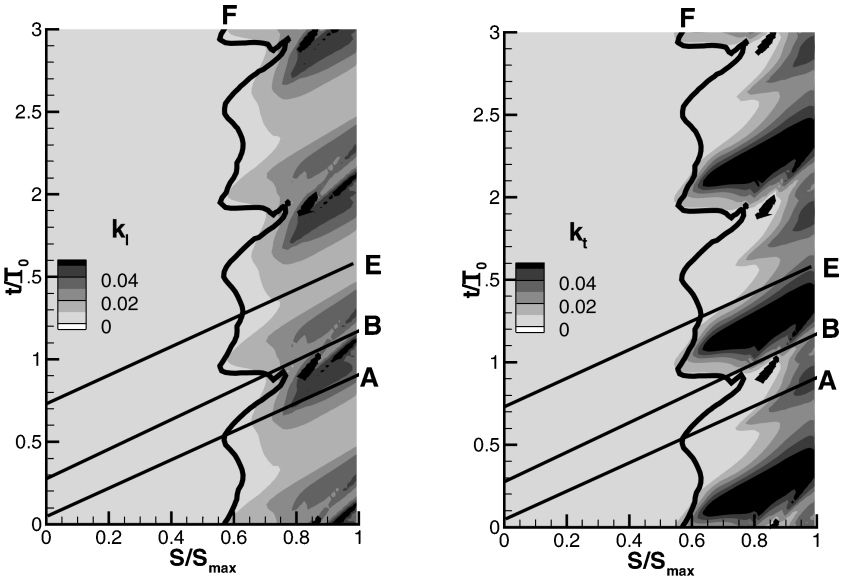

a) Laminar energy b) Turbulence energy

Fig. 6 Space–time plots of the laminar-fluctuation and turbulence energy at a distance $x/C = 0.0034$ from the suction-side surface in the boundary layer, T106A test case, $Tu = 4\%$.

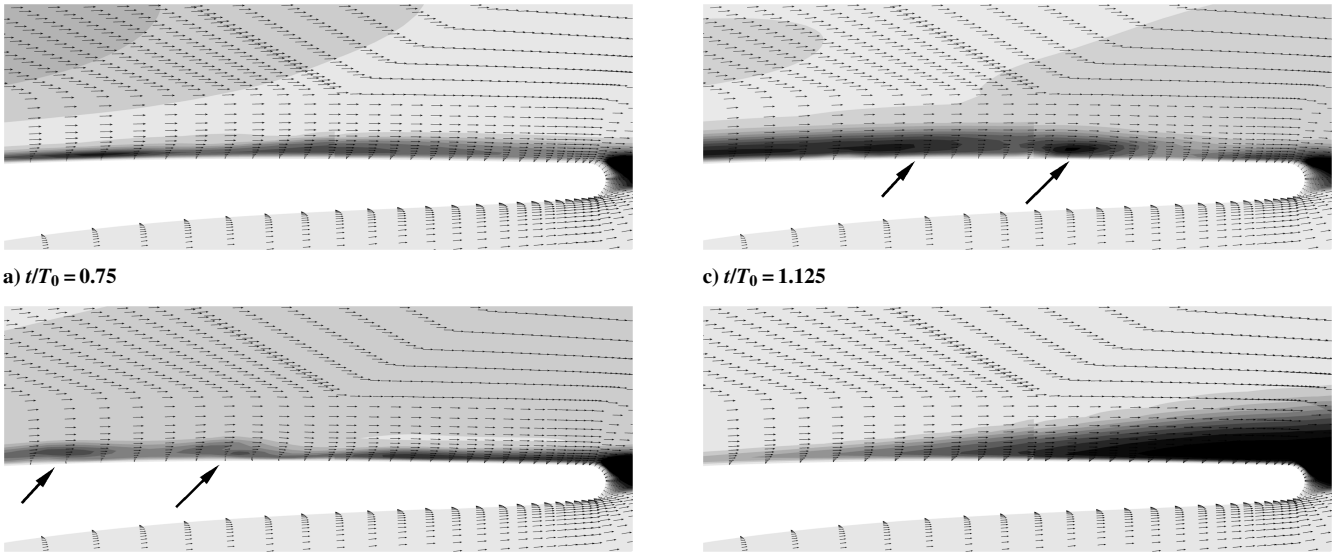

a) $t/T_0 = 0.75$ c) $t/T_0 = 1.125$

b) $t/T_0 = 1.000$ d) $t/T_0 = 1.325$

Fig. 7 Velocity vectors and shades of turbulence energy (gray scale) at four phase positions along the rear 50% of blade T106A.

according to the authors, experimental limitations prevented these small-scale, short-lifetime features from being resolved in the H-maps.

The enlargement of the separation region and the resolution of the small rollers resulting from use of the transition modification are also observed in the skin-friction maps in Fig. 5. Although the original AJL model predicts reattachement in the separation patches at around 90%, the reattachment point extends almost to the trailing edge with the transition modification included. Once separation has been suppressed by transition, at around $t/T_0 = 1$, there follows an interval $t/T_0 = 1 - 1.3$ (between lines B and E) in which the boundary is largely undisturbed (calmed), attached, and turbulent beyond $S/S_{\max} = 0.6$.

As noted earlier, one of the features of the present transition model is its ability to predict the rise of the fluctuation energy well before the rise of the skin friction. Fields of k_l and k_t, predicted at one specific wall-normal location with the transition modification, are shown in Fig. 6. The fluctuation- and the turbulence-energy components have entirely different patterns in the boundary layer. The production term of the fluctuation energy is a function of the freestream velocity and the freestream-turbulence energy, and so its level reflects directly the conditions at the boundary-layer edge. Hence, the maximum of k_l is observed between lines A and B, just downstream of the freestream peak velocity, whereas the turbulence energy k_t reaches a maximum between lines B and E, the main reason being that the rise of turbulence energy is a result (in the model) of the diffusion of freestream turbulence into the boundary layer.

Figures 7 and 8 show instantaneous views of the trailing edge of blade T106. In Fig. 7, at $t/T_0 = 1$ and $t/T_0 = 1.125$, the boundary layer clearly features short near-wall separation zones at two distinct positions (identified by arrows), already highlighted by reference to the shape-factor and skin-friction plots. As noted earlier, a similar behavior has been observed by Opoka et al.[28] and also by Stieger and Hodson,[19,20] the latter in experiments for the same blade profile, but at a freestream-turbulence intensity of 0.5%. These features just precede the transition process, which, in the computations, is probably induced by the wake turbulence alone, and this results in the elimination of the separation zone. The regions

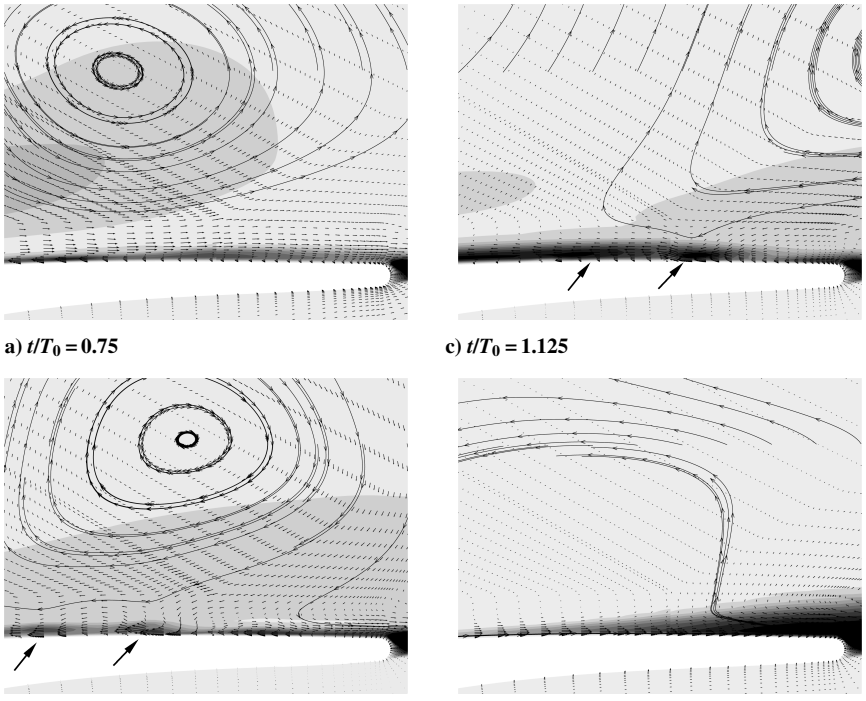

a) $t/T_0 = 0.75$ c) $t/T_0 = 1.125$

b) $t/T_0 = 1$ d) $t/T_0 = 1.325$

Fig. 8 Velocity deficit and shades of turbulence energy at four phase positions along the rear 50% of blade T106A.

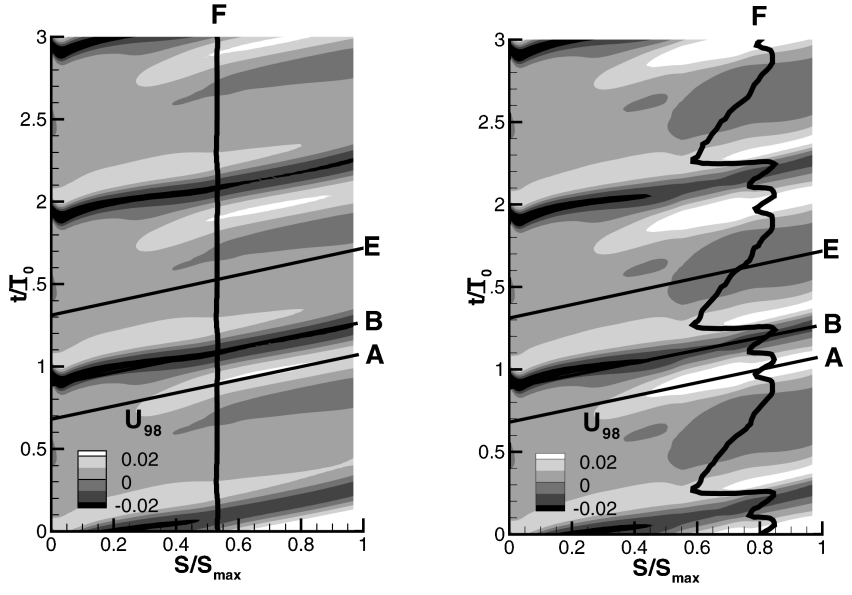

a) Original AJL model **b) Specific transition modification**

Fig. 9 Space–time plots of the velocity perturbations at the edge of the boundary layer, TC4 test case, $Tu = 4\%$.

around the two predicted separation bubbles are marked by a local elevation of the turbulence energy (dark patches), indicating a rise in turbulence generation as a consequence of high shear straining around the separation zones. Above the boundary layer, the arrival of the turbulence "cloud" in the wake is identified by dark regions.

At $t/T_0 > 1$, the wake passes across the trailing edge of the blade, enhancing transition and turbulence and eventually leading to a fully attached flow at $t/T_0 = 1.325$. Figure 8 shows the link between the negative jet—that is, the velocity deficit of the passing wake—and the two small separated regions. The streamlines are those derived from the velocity deficit and are included only to indicate the position of the negative jet, the flow defect turning anticlockwise upstream of the jet and clockwise downstream. The separation region is clearly located under the negative jet, identifying the dynamic effect of the wake on the boundary layer. Also note that these local separation regions have only been resolved because of the restriction of the time step to a very small value (800 steps per pitchwise traverse).

B. Test Case TC4

The second test case considered is blade TC4, studied experimentally by Elsner et al.[21] The experiments show that, in contrast to the preceding case, transition occurs well ahead of the trailing edge, at $S/S_{max} \approx 0.5$, and is effectively completed at $S/S_{max} \approx 0.8$. Here, the wake has a weaker effect, with unsteady features confined within the range $S/S_{max} \approx 0.5 - 0.8$.

Figure 9 shows space–time plots of the velocity perturbation at the edge of the boundary layer. Unlike in the preceding case, the

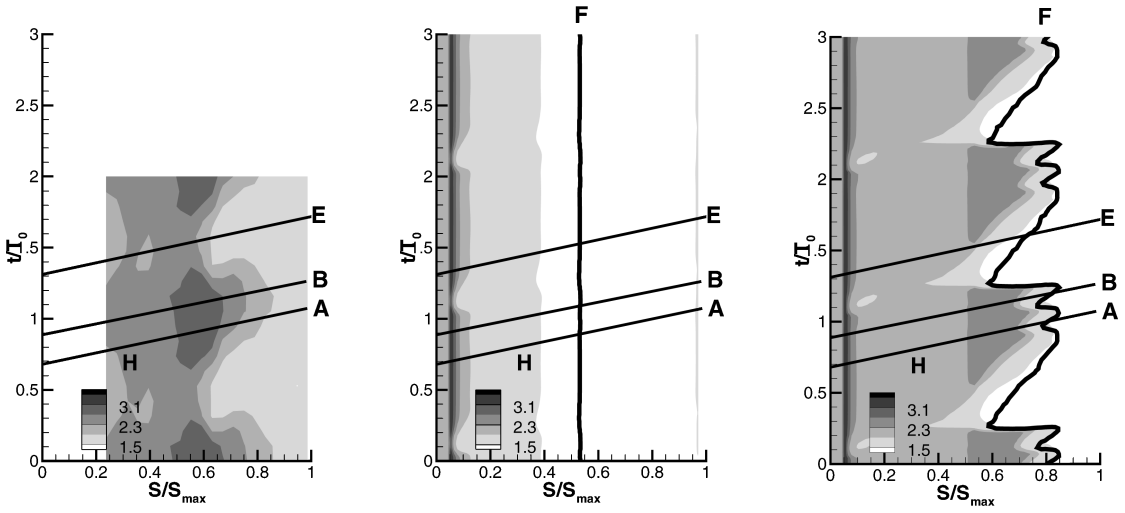

a) Experiment b) Original AJL model c) Specific transition modification

Fig. 10 Space–time plots of the shape factor H, TC4 test case, $Tu = 4\%$.

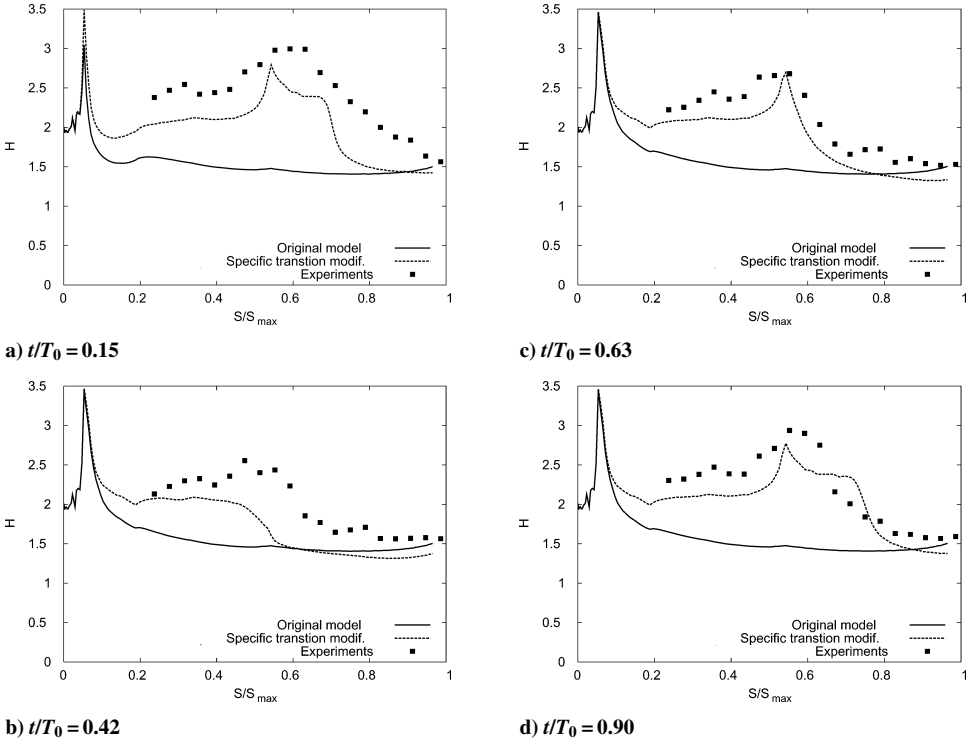

a) $t/T_0 = 0.15$ c) $t/T_0 = 0.63$

b) $t/T_0 = 0.42$ d) $t/T_0 = 0.90$

Fig. 11 Evolution of the shape factor along the TC4 blade at four phase positions.

transition modification has a substantially larger influence here on the freestream quantities, for reasons to be discussed. There is also a much larger effect of the transition modification on the locus of transition onset implied by Mayle's[7] correlation. In particular, with the original model, the onset, at $S/S_{\max} = 0.56$, is insensitive to the wakes.

The origin of this behavior may be appreciated upon reference to the space–time plots of the shape factor shown in Fig. 10. For the original AJL model, transition occurs very early, at around 15% of chord, and a fully turbulent boundary layer is established by 40% of the blade. With the boundary layer fully turbulent and relatively thick, the influence of the wakes is weak and timewise variations insignificant. Consistently, Mayle's correlation returns a transition location that is insensitive to the wakes, again because the wakes have an insignificant influence on the boundary-layer properties. Here then, the main effect of the transition modification is to substantially delay the transition onset, resulting in a behavior that is much closer to the experimental conditions. In contrast to the earlier blade, no separation occurs here, either in the experiment or the calculation. However, regions of elevated shape factor are predicted downstream of $S/S_{\max} = 0.5$ in the largely laminar region between lines A and B, as a consequence of the wake's dynamics.

Figure 11 enhances the quantitative flavor of the comparison given in Fig. 10 by presenting distributions of the shape factor along the suction side at four different time levels within one pitchwise period. The comparison demonstrates the dramatic improvement of the representation of transition achieved with the transition modification. It is recalled, with reference to Fig. 4, that the flow over blade T106 is reasonably well resolved by the basic model, in which case the transition modification has a much weaker effect. As regards the quantitative differences evident in Fig. 11, account

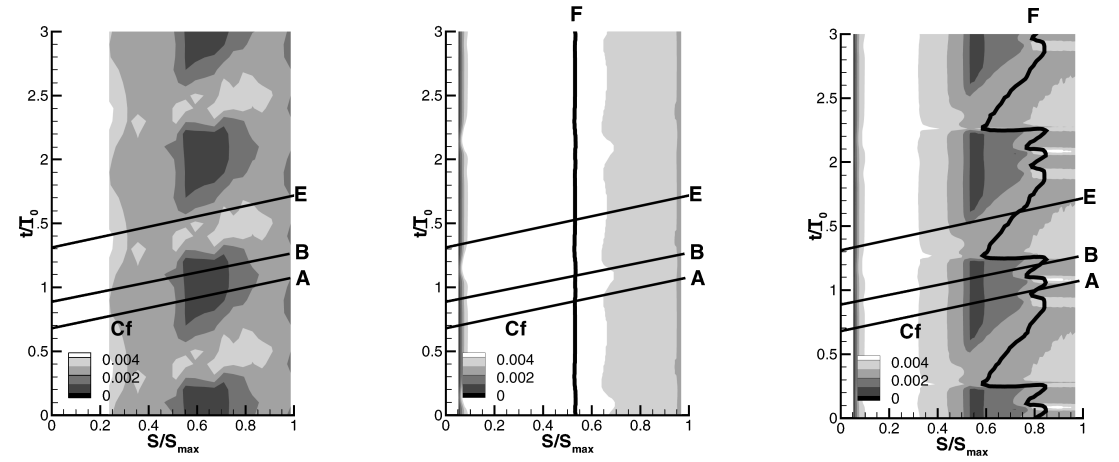

a) Experiment b) Original AJL model c) Specific transition modification

Fig. 12 Space-time plots of the skin-friction coefficient C_f, TC4 test case, $Tu = 4\%$.

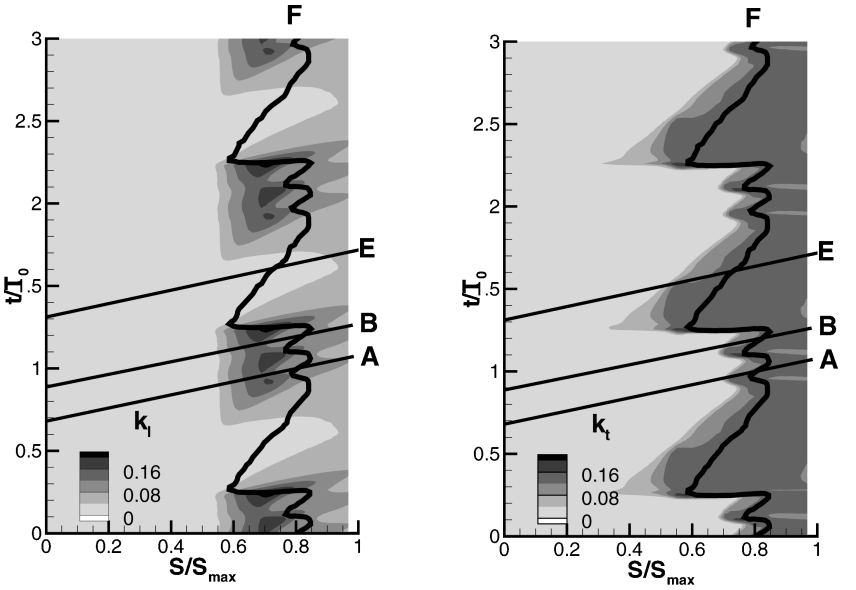

a) Laminar energy b) Turbulence energy

Fig. 13 Space–time plots of the laminar-fluctuation and turbulence energy at a distance $x/C = 0.001$ from blade in boundary layer, TC4 test case, $Tu = 4\%$.

needs to be taken of the particular difficulty of accurately determining the shape factor, both in the calculation and the experiment. Hence, the level of agreement may be claimed to be broadly satisfactory.

The agreement with the experiment is accentuated by the comparisons of the space–time variation of the skin-friction coefficient, shown in Fig. 12. As seen, regions of low C_f coincide with those in which the shape factor is high. Results for the perturbation and turbulence energy, corresponding to those given for blade T106A, are shown in Fig. 13. Very similar observations to those made earlier apply here, too: the turbulence energy rises early under the wake, in the region between lines B and E, and this gives rise to transition along the upstreammost blade-surface location; in contrast, the fluctuation energy is insignificant under the wake, but builds up between lines A and B, where the flow remains essentially laminar and approaches separation, as indicated by the low friction coefficient and high shape factor.

Instantaneous velocity-defect fields at four phase positions within one pitchwise period are shown in Fig. 14. As noted already, no separation is provoked in this case by the wake, and there is no clear evidence that can be gleaned from the experiment that the wake dynamics play, on their own, a distinctive role in the transition process.[21] Thus, it appears that the principal (perhaps, even the only) agency initiating transition is the turbulence within the wake, aided by that in the freestream. In Fig. 14, the negative jet is seen especially clearly at $t/T_0 = 0.9$, while passing the location $S/S_{\max} = 0.4$. This wake interacts with the rear of the suction side between $t/T_0 = 1.1$ and 1.5 (=0.1 and 0.5). In the region $t/T_0 = 0.9-1.15$, the boundary layer is largely laminar and thickens by virtue of the deceleration provoked within it by the wake. Figure 14a clearly shows the wake acting dynamically on the rear part of the boundary layer, and the thick layer of elevated turbulence (identified in gray) above the boundary layer signifies the presence of the turbulence cloud within the wake. It is around this instant in time that the transition location shifts drastically upstream as the rear portion of the boundary layer becomes turbulent. By $t/T_0 = 0.4$, a calmed state is established, wherein the rear boundary layer is turbulent (the dark shade in the rear 50% of the boundary layer identifying high levels of turbulence) and largely undisturbed, the wake having reached (or passed) the trailing edge. At $t/T_0 = 0.65$, the next wake is approaching the suction side, at which time the effect of the preceding wake has weakened substantially, with the transition, thus, having now moved almost to the same downstream position it had before the interaction with the previous wake.

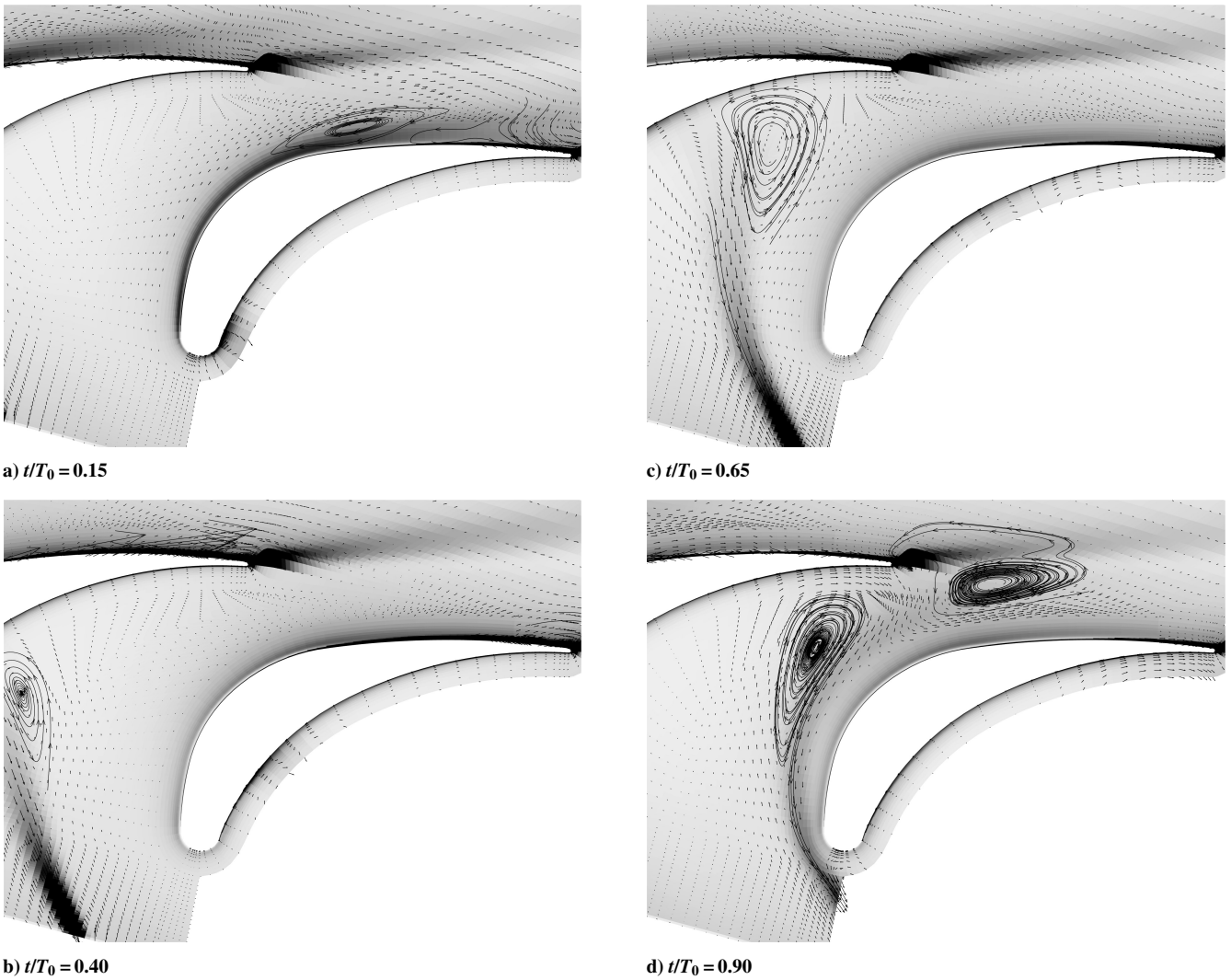

a) $t/T_0 = 0.15$ c) $t/T_0 = 0.65$

b) $t/T_0 = 0.40$ d) $t/T_0 = 0.90$

Fig. 14 Vectors of the velocity deficit and shades of the turbulence energy at four phase positions, TC4 blade, $Tu = 4\%$.

V. Conclusions

Experiments show that wake-affected transition in blade boundary layers is a complex amalgam of processes associated with the dynamics of the wakes, the unsteady transport of turbulence within them, and the turbulence in the freestream. In particular, the wake-velocity deficit can provoke an unsteady rollup process in the boundary layer that appears to cause instability and transition, independently from that effected by wake and freestream turbulence. It is difficult to counter the argument that a physically realistic description of this interaction is beyond the scope of any Reynolds-averaged Navier–Stokes (RANS) strategy. Yet, there is ample evidence, not merely in this paper, that a credible prediction of major phenomenological consequences of passing wakes on the transition process is possible by means of carefully crafted URANS methods, and it is the relative economy of such an approach, as contrasted with LES or detached eddy simulation, for example, that makes it attractive. From a practical point of view, the need to specify the wake upstream of its entry to the passage is a serious disadvantage. However, the authors have provided firm evidence in earlier papers that the inclusion of the wake-generating device within the computational process is virtually untenable, simply because the wake is seriously misrepresented within a two-dimensional URANS strategy.

With the described limitation accepted, the study demonstrates, on the basis of two entirely different blade configurations, that the principal features observed experimentally are reproduced: the wakes are predicted to cause major dynamic disturbances in the boundary layer, leading to a substantial thickening of the laminar boundary layer, in one case provoking a twin-celled separation zone, and causing the transition location initially to shift sharply downstream, between the passing wakes; transition is then provoked by a penetration of wake turbulence into the boundary layer, resulting in a substantial upstream shift in the transition location; finally, a calmed region is returned in which the boundary layer is largely undisturbed, attached, and turbulent over a significant proportion of its length. The computations reported do not only return these features, but also predict fairly well the unsteady location of the transition onset. On the negative side, there is no clear evidence that the dynamic disturbances, in themselves, induce transition. Even when these provoke separation, the eventual transition process appears to be effected solely by the penetration of turbulence into the boundary layer, in combination with high shear straining in the separated boundary layer. Although the RANS strategy should be capable, in principle, of capturing transition in the free shear layer of a separation bubble, the strong wall-induced damping the turbulence model imposes on the near-wall turbulence prevents transition when the separated zone is thin and hugs the wall, as it does in the present configuration.

Acknowledgment

The research reported in this paper was undertaken within the project Unsteady Transitional Flows in Axial Turbomachinery, funded by the European Commission under Contract G4RD-CT-2001-00628.

References

[1]Wu, X., Jacobs, R. G., Hunt, J. C. R., and Durbin, P. A., "Simulation of Boundary Layer Transition Induced by Periodically Passing Wakes," *Journal of Fluid Mechanics*, Vol. 398, 1999, pp. 109–153.

[2]Hodson, H. P., and Howell, R. J., "Bladerow Interactions, Transition and High-Lift Aerofoils in Low-Pressure turbines," *Annual Review of Fluid Mechanics*, Vol. 37, 2005, pp. 71–98.

[3]Jacobs, R. G., and Durbin, P. A., "Simulations of Bypass Transition," *Journal of Fluid Mechanics*, Vol. 428, 2001, pp. 185–212.

[4]Brandt, L., Schlatter, P., and Henningson, D. S., "Transition in Boundary Layers Subject to Free-Stream Turbulence," *Journal of Fluid Mechanics*, Vol. 517, 2004, pp. 167–198.

[5]Savill, A. M., "By-Pass Transition Using Conventional Closures," *Closure Strategies for Turbulent and Transitional Flows*, edited by B. E. Launder and N. Sandham, Cambridge Univ. Press, Cambridge, England, U.K., 2002, pp. 464–492.

[6]Savill, A. M., "New Strategies in Modelling By-Pass Transition," *Closure Strategies for Turbulent and Transitional Flows*, edited by B. E. Launder and N. Sandham, Cambridge Univ. Press, Cambridge, England, U.K., 2002, pp. 493–521.

[7]Mayle, R. E., "The Role of Laminar–Turbulent Transition in Gas Turbine Engines," *Journal of Turbomachinery*, Vol. 113, Oct. 1991, pp. 509–537.

[8]Dhawan, S., and Narasimha, R., "Some Properties of Boundary Layer During the Transition from Laminar to Turbulent Flow Motion," *Journal of Fluid Mechanics*, Vol. 3, 1958, pp. 418–436.

[9]Abu-Ghannam, B. J., and Shaw, R., "Natural Transition of Boundary Layers—the Effect of Turbulence, Pressure Gradient and Flow History," *Journal of Mechanical Engineering Science*, Vol. 22, No. 5, 1980, pp. 213–228.

[10]Cho, J. R., and Chung, M. K., "A $k-\varepsilon-\gamma$ Equation Turbulence Model," *Journal of Fluid Mechanics*, Vol. 237, 1992, pp. 301–322.

[11]Steelant, J., and Dick, E., "Modelling of Bypass Transition with Conditioned Navier–Stokes Equations Coupled to an Intermittency Transport Equation," *International Journal of Numerical Methods in Fluids*, Vol. 23, No. 3, 1996, pp. 193–220.

[12]Steelant, J., and Dick, E., "Modelling of Laminar–Turbulent Transition for High Freestream Turbulence," *Journal of Fluids Engineering*, Vol. 123, No. 3, 2001, pp. 22–30.

[13]Suzen, Y. B., and Huang, P. G., "Modelling of Flow Transition Using an Intermittency Transport Equation," *Journal of Fluids Engineering*, Vol. 122, No. 2, 2000, pp. 273–284.

[14]Vicedo, J., Vilmin, S., Dawes, W. N., and Savill, A. M., "Intermittency Transport Modeling of Separated Flow Transition," *Journal of Turbomachinery*, Vol. 126, 2004, pp. 424–431.

[15]Higazy, M. G., "Numerical Prediction of Transition Boundary-Layer Flows Using New Intermittency Transport Equation," *Aeronautical Journal*, Vol. 106, June 2002, p. 1060.

[16]Lardeau, S., Leschziner, M. A., and Li, N., "Modelling Bypass Transition with Low-Reynolds-Number Nonlinear Eddy-Viscosity Closure," *Flow, Turbulence and Combustion*, Vol. 73, No. 1, 2004, pp. 49–76.

[17]Abe, K., Jang, Y.-J., and Leschziner, M. A., "An Investigation of Wall-Anisotropy Expressions and Length-Scale for Non-Linear Eddy-Viscosity Models," *International Journal of Heat and Fluid Flow*, Vol. 28, No. 2, 2002, pp. 181–198.

[18]Lardeau, S., and Leschziner, M. A., "Unsteady RANS Modelling of Wake–Blade Interaction: Computational Requirements and Limitations," *Computers and Fluids*, Vol. 34, No. 1, 2005, pp. 3–21.

[19]Stieger, R. D., and Hodson, H. P., "Unsteady Surface Pressures Due to Wake Induced Transition in a Laminar Separation Bubble on a LP Turbine Cascade," *ASME Turbo Expo, Power for Land, Sea and Air*, American Society of Mechanical Engineers, 2003.

[20]Stieger, R. D., and Hodson, H. P., "The Transition Mechanism of Highly-Loaded LP Turbine Blades," *ASME Turbo Expo, Power for Land, Sea and Air*, American Society of Mechanical Engineers, 2003.

[21]Elsner, W., Vilmin, S., Drobniak, S., and Piotrowski, W., "Experimental Analysis and Prediction of Wake-Induced Transition in Turbomachinery," American Society of Mechanical Engineers, ASME Paper GT2004-53757, June 2004.

[22]Wang, C., Jang, Y.-J., and Leschziner, M. A., "Modelling Two- and Three-Dimensional Curved Surfaces with Anisotropy-Resolving Turbulence Closures," *International Journal of Heat and Fluid Flow*, Vol. 25, No. 3, 2004, pp. 499–512.

[23]Mayle, R. E., and Schulz, A., "The Path to Predicting Bypass Transition," *Journal of Turbomachinery*, Vol. 119, No. 3, 1997, pp. 405–411.

[24]Lardeau, S., and Leschziner, M. A., "Unsteady RANS Computations of Transitional Wake-Blade Interaction," *AIAA Journal*, Vol. 42, No. 8, 2004, pp. 1559–1571.

[25]Lien, F. S., Chen, W. L., and Leschziner, M. A., "A Multiblock Implementation of a Non-Orthogonal Collocated Finite Volume Algorithm for Complex Turbulent Flows," *International Journal of Numerical Methods in Fluids*, Vol. 23, No. 6, 1996, pp. 567–588.

[26]Chen, W.-L., and Leschziner, M. A., "Turbulence Modelling of Rotor–Stator Interaction with Linear and Non-linear Eddy-Viscosity Models," *Proceedings of the 3rd European Conference on Turbomachinery–Fluid Dynamics and Thermodynamics*, Institution of Mechanical Engineers Conf. Transaction, 1999, pp. 259–270.

[27]Lien, F. S., and Leschziner, M. A., "A General Non-Orthogonal Collocated Finite Volume Algorithm for Turbulent Flow at All Speeds Incorporating Second-Moment Turbulence-Transport Closure, Part 1: Computational Implementation," *Computational Methods in Applied Mechanical Engineering*, Vol. 114, Jan. 1994, pp. 123–148.

[28]Opoka, M., and Hodson, H., "Experimental Investigation and Numerical Predictions of the Unsteady Transition Process on the High Lift T106a Turbine Blade," 17th ISABE Symposium, ISABE-2005-1277, Munich, Sept. 2005.

[29]Wilcox, D. C., "Turbulence Modelling for CFD," DCW Industries, 1998.

K. Ghia
Associate Editor